Volume 14 | Number 3 | 7 February 2014 | Pages 433–610

Lab on a Chip

Miniaturisation for chemistry, physics, biology, materials science and bioengineering

www.rsc.org/loc

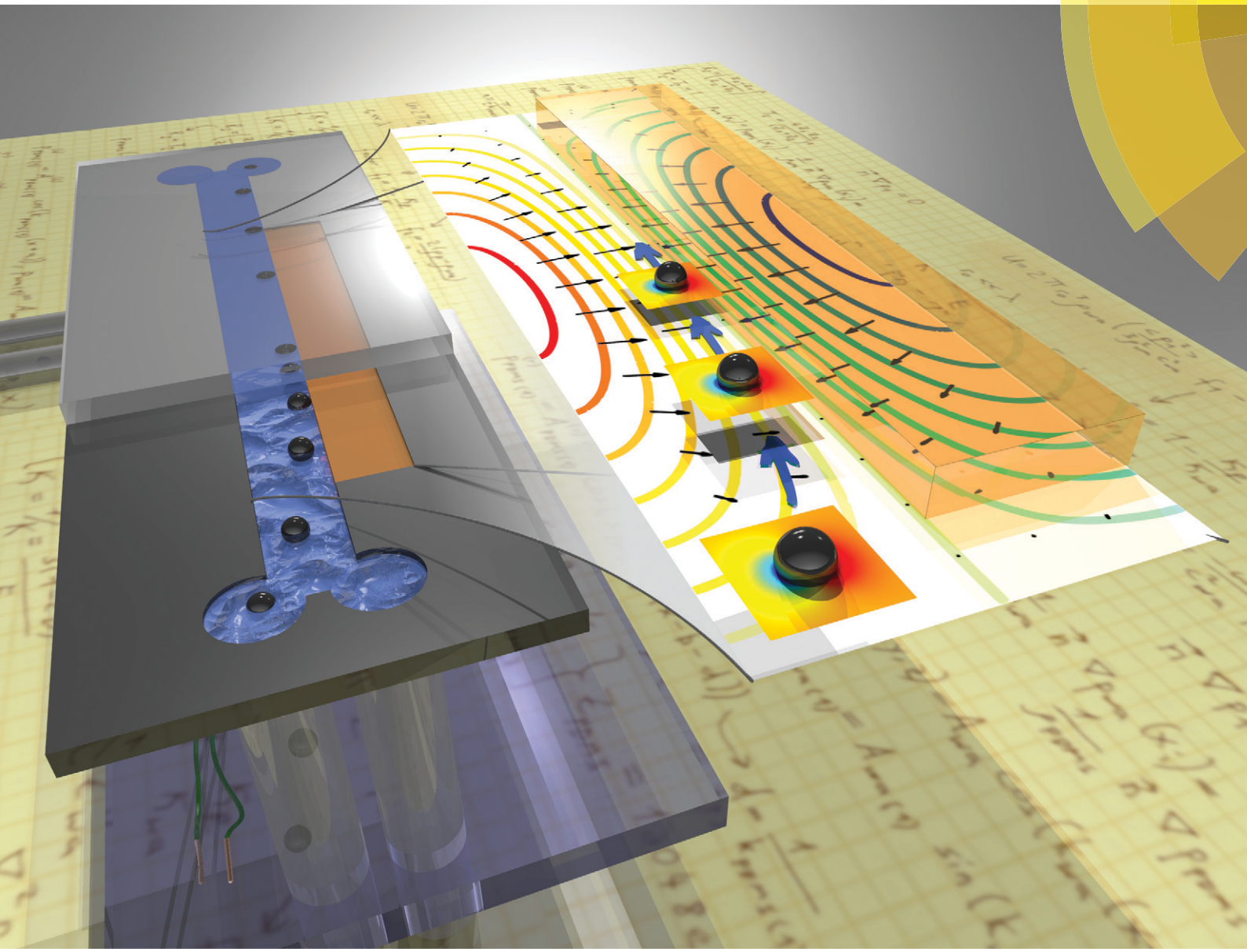

ISSN 1473-0197

ROYAL SOCIETY OF CHEMISTRY

PAPER
Ivo Leibacher *et al.*
Impedance matched channel walls in acoustofluidic systems

Lab on a Chip

PAPER

View Article Online
View Journal | View Issue

Cite this: *Lab Chip*, 2014, **14**, 463

Impedance matched channel walls in acoustofluidic systems†

Ivo Leibacher,* Sebastian Schatzer and Jürg Dual

Acoustophoresis in bulk acoustic wave (BAW) devices typically operates with an ultrasonic standing wave in a microfluidic channel between two opposing silicon walls, which act as both the acoustic and the fluidic boundary. In this paper, we describe BAW devices with an additional material layer of polydimethylsiloxane (PDMS). This PDMS wall is introduced to decouple the acoustic boundary (silicon wall) from the fluidic boundary (PDMS wall) by acoustic impedance matching. The acoustic field and the resulting particle manipulation are thereby less restricted than in conventional BAW devices. In the presented devices, particle accumulation lines can be placed arbitrarily within the fluidic domain, which strongly increases the possibility of acoustophoresis. The paper covers experimental results, an analytical model in good agreement and microfabrication techniques for PDMS enclosed in a microchannel. An application example for microparticle concentration is demonstrated. The presented approach offers further potential for biotechnological applications such as particle separation, enhanced particle sensors and cell handling.

Received 30th September 2013,
Accepted 11th November 2013

DOI: 10.1039/c3lc51109j

www.rsc.org/loc

1. Introduction

The movement of microparticles by forces of an acoustic field, namely acoustophoresis or ultrasonic particle manipulation, holds significant promise for emerging applications in bio- and microtechnological lab-on-a-chip systems. Acoustofluidic devices enable microfluidic operations such as the handling,[1] positioning,[2] separation[3] and characterization[4] of cell-sized microparticles and biological cells, as recently reviewed in a series of 23 tutorials in *Lab on a Chip*.[5]

A basic configuration for acoustophoresis in bulk acoustic wave (BAW) devices consists of a fluidic channel with two parallel, opposing walls as reviewed by Lenshof *et al.*[6] In such a configuration, the silicon walls fulfill two tasks. Firstly, they are the *fluidic boundary* for the flow. Secondly, the opposing parallel walls are *reflectors* for the propagating waves in the fluid and thus cause the generation of an ultrasonic standing wave. This results from the superposition of an incident and a reflected propagating wave. This double role leads inherently to restrictions for the ultrasonic field. As presented in this paper and illustrated in Fig. 1, channels with additional boundary materials can overcome such limitations. By decoupling the two wall assignments, our design[7] allows arbitrary placement of the pressure nodal lines relative to the fluidic walls. We impose such a boundary by an additional polydimethylsiloxane (PDMS) layer in the device as shown in Fig. 2. PDMS is chosen because its impedance matches the impedance of water quite well, and it is a widely used material in microfluidics with excellent biocompatibility and fabrication properties.

A key feature of the devices reported here is the ability to attract particles (with positive acoustic contrast factor) to a wall in a micro-electro-mechanical system (MEMS). This is not possible in common acoustophoretic devices with silicon boundaries, since they result in a pressure maximum on the wall as in Fig. 1. The ability to push particles or cells on a microfluidic channel wall has significant biotechnological relevance when the attracting walls are coated sensor surfaces, as recently outlined in the review of Wiklund *et al.*[8] For example, particles can be pushed acoustophoretically on a wall coated with immuno-selective agents, where only selected particles are bound and detected in a subsequent sensing step. Furthermore, thinking in terms of applications of particle-attracting microchannel walls, we present an on-chip particle concentration experiment.

Existing methods to attract particles to a wall (such as quarter-wavelength resonators)[9] are experimentally challenging. This has encouraged the search for more robust alternatives. One example is the thin reflector design of Glynne-Jones *et al.*[10]

Institute of Mechanical Systems (IMES), Department of Mechanical and Process Engineering, Swiss Federal Institute of Technology (ETH Zurich), Tannenstrasse 3, CH-8092 Zurich, Switzerland. E-mail: leibacher@imes.mavt.ethz.ch; Tel: +41 44 632 5293

† Electronic supplementary information (ESI) available: Experimental video of microfluidic particle concentration with PDMS boundaries (Fig. 11). See DOI: 10.1039/c3lc51109j

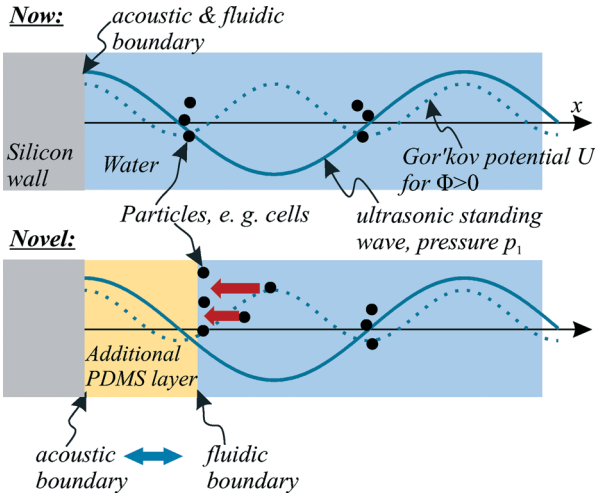

Fig. 1 Illustration of the impedance matching concept with PDMS. The materials silicon, PDMS and water across a microfluidic channel are shown, together with the pressure distribution (solid line) and a Gor'kov potential for $\Phi > 0$ (dotted line, eqn (1)).

Moreover, Ding *et al.*[11] showed that acoustophoresis with surface acoustic wave (SAW) devices also allows arbitrary placement of pressure nodal lines. The method presented in our work offers a novel approach, whose microtechnological realisation and geometrical configuration differ from previous work. Our method gives higher freedom for the design of devices in general while maintaining a simple piezoelectric excitation setup with a lower typical frequency range compared to SAW devices.

In this paper, we first present a theoretical model which coincides well with the following microfluidic experiments. We investigate both proof of concept and application-oriented experiments.

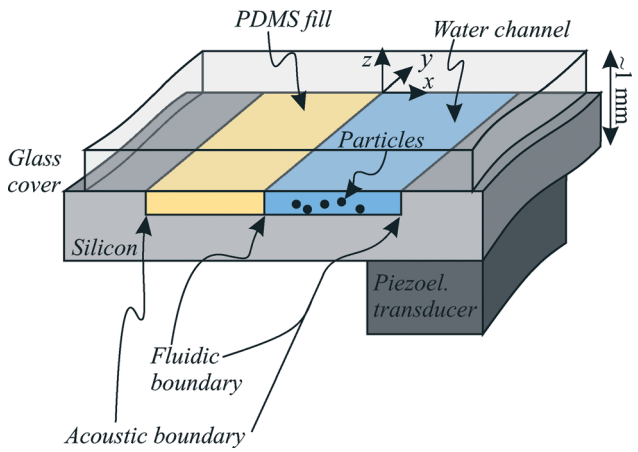

Fig. 2 Sketch of a microfluidic device section. A channel in the *y*-direction is partially filled with water and PDMS. Regarding the pressure field within the water channel, the PDMS fill gives an additional degree of freedom for acoustophoresis on the suspended particles.

2. Theoretical background

2.1. Basic equations

The basic equations for the calculation of acoustophoretic forces on particles are recapitulated in the following.

The Gor'kov potential[12] U in the acoustic domain reads:

$$U = 2\pi r_o^3 \rho_{wa} \left(\frac{\langle p_1^2 \rangle}{3\rho_{wa}^2 c_{wa}^2} f_1 - \frac{\langle v_1^2 \rangle}{2} f_2 \right) \quad (1)$$

with the particle radius r_o, the density ρ_{wa}, the speed of sound c_{wa} in the fluid (here water), the first-order pressure and velocity fields p_1 and v_1 and the material-dependent factors f_1 and f_2. ρ_{wa} is the density of water in the quiescent state (namely the zero order density ρ_0). v_1 describes the magnitude of the real part of the complex velocity field vector (phasor), $v_1 = \|\mathrm{Re}(\mathbf{v}_1)\|$. Time averaging is denoted by $\langle . \rangle$. The Gor'kov potential is valid for particles with $r_o \ll \lambda$ with the acoustic wavelength λ, in other words, in the long-wavelength range. Particles in the acoustic domain are attracted to the minimum of the Gor'kov potential U. The acoustic radiation force $\mathbf{F}$ on a particle is equal to

$$\mathbf{F} = -\nabla U \quad (2)$$

The first factor f_1 is given by

$$f_1 = 1 - \frac{\kappa_p}{\kappa_{wa}} \quad (3)$$

with the compressibility κ and the indices "p" for the particle material and "wa" for the surrounding water. For fluids, the compressibility is calculated as

$$\kappa = \frac{1}{\rho c^2} \quad (4)$$

which is sometimes also taken as a rough approximation for solids with low shear modulus. More precisely, for a solid, its compressibility is the inverse of the bulk modulus K of elasticity:

$$\kappa = \frac{1}{K} = \frac{3(1-2\nu)}{E} \quad (5)$$

with Young's modulus E and Poisson's ratio ν.

The second factor f_2 determines the influence of the velocity field in the Gor'kov potential. With the densities ρ, it is given as

$$f_2 = \frac{2(\rho_p - \rho_{wa})}{2\rho_p + \rho_{wa}} \quad (6)$$

A common value to characterize the particle behavior in a one-dimensional ultrasonic standing wave is the acoustophoretic contrast factor[13] $\Phi = \frac{f_1}{3} + \frac{f_2}{2}$. As discussed in the literature,[14,15] particles with $\Phi > 0$ are attracted to the nodes of p_1 (pressure nodes) according to Gor'kov's equation. These pressure nodes

are also the antinodes of v_1. *Vice versa*, particles with $\Phi < 0$ are attracted to the antinodes of p_1, which correspond to the nodes of v_1. In other words, particles get attracted to the minima of the potential field U, as qualitatively illustrated in Fig. 1. For $\Phi > 0$, the minima of U correspond to the pressure nodes, whereas for $\Phi < 0$, the minima of U correspond to the pressure antinodes. Most common particles (*e.g.* glass, polystyrene, cells) exhibit $\Phi > 0$. Therefore, in this paper, we are mostly calculating in terms of p_1 in order to find the pressure nodes which denote the particle collection points.

The fundamental Helmholtz equation

$$\nabla^2 p_1 = \frac{-\omega^2}{c_{\mathrm{wa}}^2} p_1 \tag{7}$$

describes the pressure field within an acoustic domain, where time-harmonic fields are implicitly assumed:

$$p_1 = p_1(x)\mathrm{e}^{-\mathrm{i}\omega t} \tag{8}$$

The first-order velocity and density fields follow from the pressure field.[16]

The boundary conditions at the border of an acoustic domain depend on the characteristic acoustic impedance $Z = \rho c$ of the domain itself and its adjacent domains, as illustrated in Fig. 3. The intensity reflection coefficient R_I and the intensity transmission coefficient T_I describe the behavior of an acoustic traveling wave at an interface between two materials with indices 1 and 2 (for normal incidence):[17]

$$R_\mathrm{I} = \left(\frac{Z_2 - Z_1}{Z_2 + Z_1}\right)^2, \quad T_\mathrm{I} = \frac{4Z_1Z_2}{(Z_1 + Z_2)^2} \tag{9}$$

Their sum gives $R_\mathrm{I} + T_\mathrm{I} = 1$, which signifies conservation of energy. These coefficients are meaningful in our problem because an ultrasonic standing wave can be seen as the superposition of an incident traveling wave with its counter-propagating reflected wave which originates from a reflecting boundary. For the high impedance mismatch $Z_{\mathrm{si}} \gg Z_{\mathrm{wa}}$ between the silicon wall and the water (see Table 1), $R_\mathrm{I} = 0.75$ and $T_\mathrm{I} = 0.25$ denote that the energy of an incident wave will mostly be reflected at this interface. Similarly, a silicon–PDMS interface has $R_\mathrm{I} = 0.82$ and $T_\mathrm{I} = 0.18$ as will be discussed in section 3.1. In these cases, even though the reflection is not perfect, as commonly experienced from experiments, the so-called hard-wall condition[16] with zero wall velocity gives a valid boundary modeling:

$$\mathbf{n}\cdot\nabla p_1 = 0 \tag{10}$$

with the normal vector $\mathbf{n}$ on the wall surface. This hard-wall boundary condition can only be fulfilled with a pressure antinode at the wall surface (see Fig. 1), which is the reason why particles cannot be attracted to silicon walls in microfluidic systems.

For the interface between two materials with similar Z, such as a PDMS–water interface with the PDMS impedance $Z_\pi \approx Z_{\mathrm{wa}}$, we expect mostly transmission and negligible reflection since $T_\mathrm{I} = 0.97$ and $R_\mathrm{I} = 0.03$. At such an interface, we write the continuity condition for pressure

$$p_{\mathrm{wa}}(x_\mathrm{i}) = p_\pi(x_\mathrm{i}) \tag{11}$$

and the continuity condition for velocity[16]

$$\frac{1}{\rho_{\mathrm{wa}}}\mathbf{n}\cdot\nabla p_{\mathrm{wa}}(x_\mathrm{i}) = \frac{1}{\rho_\pi}\mathbf{n}\cdot\nabla p_\pi(x_\mathrm{i}) \tag{12}$$

with the coordinate x_i of the interface. p_{wa} and p_π denote the first-order pressure p_1 in water and PDMS.

2.2 Standing waves in PDMS-filled microfluidic channels

Here we discuss a microfluidic channel with two opposing silicon walls parallel to the yz-plane as in Fig. 2, between which a PDMS layer and a water layer are placed. First, our aim is to model an ultrasonic standing wave in the x-direction with its pressure node on the interface between the PDMS and the water at $x = 0$, as plotted in Fig. 4. In this configuration, the pressure node will attract particles to the PDMS wall (marked as "collection point"). The pressure field in the PDMS (index π) and in the water (index wa) reads:

$$p_\pi(x,y,z) = A_\pi \sin(k_\pi x) \tag{13}$$

$$p_{\mathrm{wa}}(x,y,z) = A_{\mathrm{wa}} \cos(k_{\mathrm{wa}}(x - b)) \tag{14}$$

where a and b are the widths of the PDMS and water in the x-direction, and $k = \omega/c_{\mathrm{sound}} = 2\pi/\lambda$ is the wave number in the respective medium.

When we design a water channel of width b, the plotted first resonance mode has $\lambda_{\mathrm{wa}}/4$ in the water domain. It occurs at a frequency of $f_{(1)} = c_{\mathrm{wa}}/\lambda_{\mathrm{wa}} = c_{\mathrm{wa}}/(4b)$. Consequently, the PDMS width has to be $a = \lambda_\pi/4 = c_\pi/(4f_{(1)})$, so p_π fulfills the hard-wall boundary condition of eqn (10) on the left wall. The hard-wall condition on the right wall is already fulfilled by the chosen p_{wa} of eqn (14). In this configuration, the ratio $a/b = c_\pi/c_{\mathrm{wa}} \approx 0.68$ follows according to Table 1. Finally, the amplitude ratio A_{wa}/A_π was calculated using eqn (12), resulting in the plot shown in Fig. 4.

By varying the PDMS layer thickness a, the position x_0 of the particle-attracting pressure nodal line can be moved.

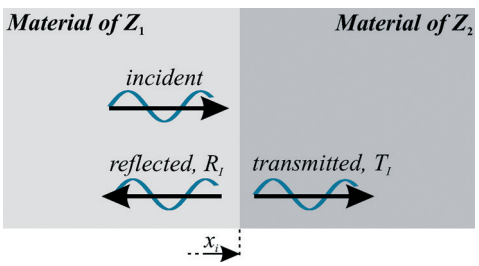

Fig. 3 Wave propagation at the interface between two materials.

Table 1 Material parameters for the calculation of characteristic acoustic impedances

Material	Speed of sound	Density	Characteristic acoustic impedance $Z = c\rho$
PDMS	$c_\pi = 1019$ m s^{-1}	$\rho_\pi = 1028$ kg m^{-3}	$Z_\pi = 1.048 \times 10^6$ Ns m^{-3}
Water[16]	$c_{wa} = 1497$ m s^{-1}	$\rho_{wa} = 998$ kg m^{-3}	$Z_{wa} = 1.494 \times 10^6$ Ns m^{-3}
Isopropanol[22]	$c_{is} = 1139$ m s^{-1}	$\rho_{is} = 781$ kg m^{-3}	$Z_{is} = 0.890 \times 10^6$ Ns m^{-3}
Silicon,[16,23] [110] direction	$c_{si} = 9133$ m s^{-1}	$\rho_{si} = 2331$ kg m^{-3}	$Z_{si} = 21.289 \times 10^6$ Ns m^{-3}

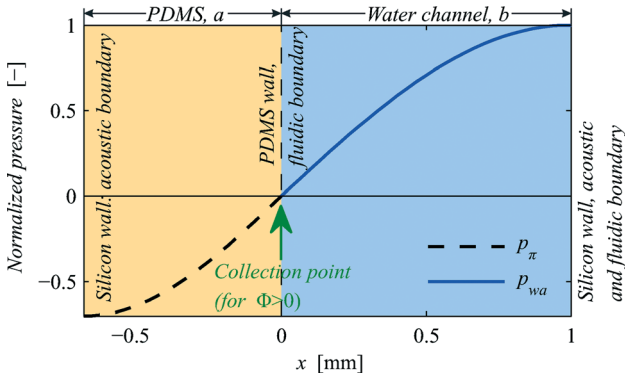

Fig. 4 Pressure plot in a microfluidic PDMS/water channel cross-section with a $\lambda/2$ standing wave (first eigenmode). Particles with $\Phi > 0$ are attracted to the marked collection point at the PDMS wall. With the water channel width b = 1 mm, this mode occurs at 374 kHz.

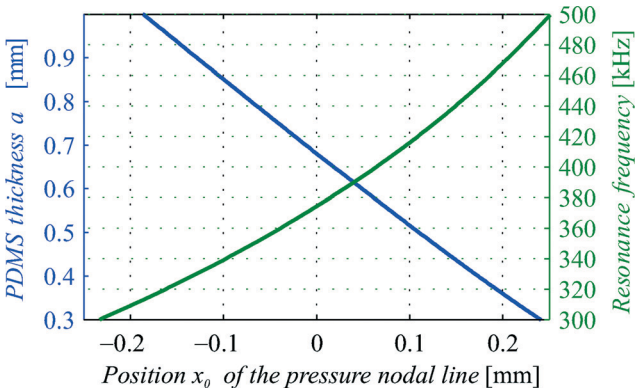

Fig. 5 For the $\lambda/2$ mode as in Fig. 4 with a water channel width b = 1 mm, the PDMS thickness a as well as the resonance frequency are given depending on the position x_0 (design parameter) of the pressure node (= particle collection point). Fig. 4 represents the solution for $x_0 = 0$.

Qualitatively speaking, by increasing a, the pressure nodal line is moved to the left within the PDMS layer ($x_0 < 0$), and the resonance frequency for the $\lambda/2$ mode decreases. Such a configuration can be beneficial because the particles on the PDMS wall continue to experience a force towards the wall, unlike the situation in Fig. 4, where the particles on the PDMS at $x = 0$ experience zero acoustic radiation force since they are located at a minimum of U with $\mathbf{F}(x = 0) = -\nabla U(x = 0) = 0$. By decreasing the PDMS thickness a, the pressure nodal line is moved rightwards to $x_0 > 0$ within the water layer, and the resonance frequency rises. This configuration is beneficial for flow-through applications, where particles would get stuck at $x = 0$ in Fig. 4 because of zero flow velocity according to the fluidic no slip condition at the wall. An analytical calculation of these considerations is plotted in Fig. 5. As an alternative to these analytical calculations, by using an acoustic simulation *e.g.* in Comsol Multiphysics®, the same results can be simulated. Numerical models also allow the presentation of the influence of the fluidic inlet and outlet on the acoustic field.

In the following, another device configuration will be discussed. Fig. 6 shows the pressure plot for a water channel in between *two* PDMS layers. The PDMS thicknesses a and d were calculated to reach the following result: in the $\lambda/2$ mode (first eigenmode), the particles are collected on the left water channel wall (collection point 1), whereas in the λ mode (second eigenmode), suspended particles are collected on the right channel wall (collection point 2). Such a design has potential applications for switching a particle flow on a junction in a similar manner as described by Laurell *et al.*[3] Another application lies in the focusing of particles on a line with an arbitrary x-coordinate, when mode-switching is considered.[18]

The transverse $\lambda/2$ mode in Fig. 6 is based on the following analytical functions:

$$p^{(l)}_{\pi(1)} = A^{(l)}_{\pi(1)} \cos(k_{\pi(1)}(x + a)) \quad (15)$$

$$p_{wa(1)} = A_{wa(1)} \sin(k_{wa(1)}x) \quad (16)$$

$$p^{(r)}_{\pi(1)} = A^{(r)}_{\pi(1)} \cos(k_{\pi(1)}(x - b - d)) \quad (17)$$

where the superscript "l" refers to the left and "r" refers to the right PDMS layer. The subscript 1 refers to the first

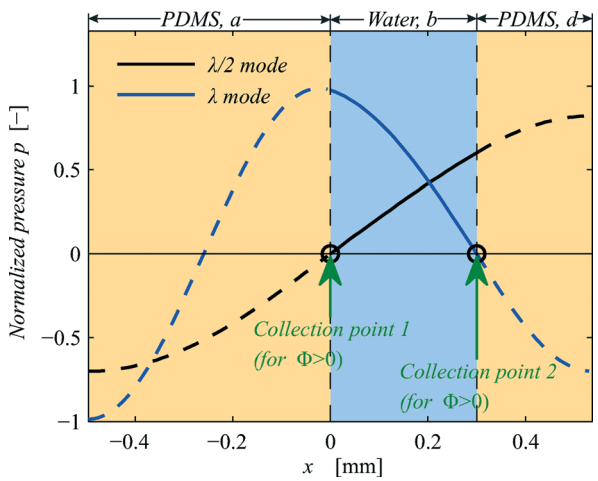

Fig. 6 Pressure plot of the first and second eigenmodes in a PDMS/water/PDMS channel cross-section. The $\lambda/2$ mode occurs at 513 kHz, the λ mode at 1076 kHz for the given water channel width b = 300 μm.

resonance mode with $\lambda/2$ across the channel. For the second resonance mode, the λ mode, we write:

$$p^{(l)}_{\pi(2)} = A^{(l)}_{\pi(2)} \cos(k_{\pi(2)}(x + a)) \quad (18)$$

$$p_{wa(2)} = A_{wa(2)} \sin(k_{wa(2)}(x - b)) \quad (19)$$

$$p^{(r)}_{\pi(2)} = A^{(r)}_{\pi(2)} \sin(k_{\pi(2)}(x - b)) \quad (20)$$

Several of the 6 boundary conditions at $x = -a$, $x = 0$, $x = b$ and $x = b + d$ are already satisfied by the chosen functions above. Still these functions have to fulfill eqn (11) and (12) at $x = b$ in the $\lambda/2$ mode and at $x = 0$ in the λ mode. After insertion, dividing eqn (11) by eqn (12) gives

$$d = \frac{1}{k_{\pi(1)}} \arctan\left(\frac{\rho_\pi k_{wa(1)}}{\rho_{wa} k_{\pi(1)}} \frac{1}{\tan\left(k_{wa(1)} b\right)} \right) \quad (21)$$

$$a = \frac{1}{k_{\pi(2)}} \arctan\left(\frac{\rho_\pi k_{wa(2)}}{\rho_{wa} k_{\pi(2)}} \frac{1}{\tan\left(k_{wa(2)} b\right)} \right) \quad (22)$$

Furthermore, we have

$$a = \frac{\pi}{2k_{\pi(1)}}, \quad d = \frac{\pi}{2k_{\pi(2)}} \quad (23)$$

The eigenmode solution which is plotted in Fig. 6 was found in a plot over the a- and d-parameters. The thicknesses have to be chosen with a ratio $a : b : d = 1.65 : 1 : 0.79$ to achieve the configuration shown in the plot.

3. Experiments

3.1 Measurement of the longitudinal wave speed c_π in PDMS

The mechanical properties of PDMS might vary depending on the manufacturer and curing method. Therefore, we fabricated a PDMS block exactly the same way as in the device fabrication process for the subsequent measurement of c_π as listed in Table 1. We fabricated the PDMS bulk block of Dow Corning Sylgard® 184 and measured the pulse-echo time Δt using an Olympus Panametrics 5800PR as plotted in Fig. 7. For both 1 MHz and 5 MHz transceivers for longitudinal waves, our measurements averaged to 1019 m s^{-1}. Hartmann and Jarzynski[19] reported c_π = 1020 m s^{-1} at 0.6 MHz. This leads to the conclusion that c_π is rather independent of frequency in our ultrasonic range. Furthermore, this measurement shows that the material damping of PDMS is not prohibitory for the propagation of longitudinal waves. Together with the density ρ_π = 1028 kg m^{-3}, PDMS yields an acoustic impedance $Z_\pi = 1.048 \times 10^6$ Ns m^{-3}, which is 30% lower than water. With this impedance, for a PDMS–silicon interface, we obtain R_I = 0.82 and T_I = 0.18 from eqn (9), which denotes mostly reflection of incident waves. However, at a PDMS–water interface with R_I = 0.03 and T_I = 0.97, 97% of the intensity of the wave will be transmitted, which will be seen to give the expected impedance matching performance. Alternatively, materials other than PDMS might prove to be even more suitable when their characteristic acoustic impedance is closer to that of water. This is the case *e.g.* for the rho-c materials of Acoustic Polymers Ltd., which might be used if the manufacturing procedures can be resolved.

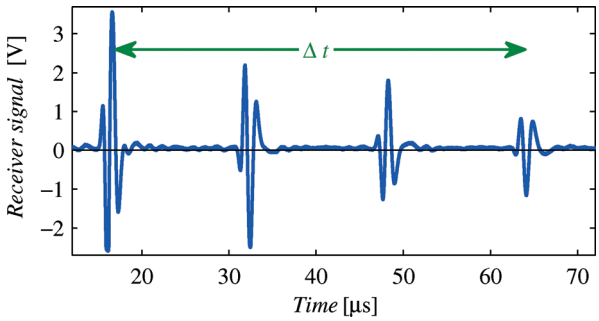

Fig. 7 Four pulse-echoes from a longitudinal wave in a bulk PDMS sample of 8.15 mm thickness, measured with a 1 MHz transceiver. This measurement allows calculation of the speed of sound c_π and estimation of the material damping.

For a complete linear elastic characterization of PDMS, we also tried to measure the transverse wave speed of PDMS using shear transceivers. Whereas this method works well for metals and stiffer polymers, for PDMS, we could not measure an echo of a transverse wave. Most probably the damping of transverse waves is very high in this case, hindering the propagation of transverse waves in PDMS.

3.2. Device fabrication and experimental setup

The devices were fabricated on a silicon wafer (thickness 425 μm, polished on both sides). As illustrated in step (a) in Fig. 9, microfluidic channels were dry etched (60 μm–150 μm) in the silicon substrate using an inductive coupled plasma system. The wafer was then diced to the device size of 24 mm × 8 mm. Freshly mixed and therefore liquid PDMS was poured on these devices. In step (b), a silicon cover plate was put on top to squeeze out excess PDMS and to obtain a flat, levelled top side of the PDMS. A weight of ~0.025 kg was placed on top of the cover plate to exert a slight force in the negative z-direction. Before step (b), the cover plates were laid in a closed chamber next to some drops of evaporating chlorotrimethylsilane (silanizing agent) for 30 min to obtain a non-stick surface. After curing the PDMS for 3 days at room temperature, the cover plates were released. In step (c), the PDMS was cut using a laser mill (New Wave Research).[20] We preferred cutting the PDMS using the laser because it is more precise than cutting by hand using a knife. The laser cutting results in a PDMS wall which is still not perfectly vertical, and the induced heating might affect the PDMS. However, these imperfections were found to be small compared to the PDMS width and the wavelength. After cutting, spare PDMS parts were removed by means of a syringe tip. Finally, the device was covered with a glass plate (thickness 500 μm) in step (d). The glass plate was

bonded by applying a very small amount of liquid PDMS between the two surfaces. A photo of the device is given in Fig. 8.

For the actuation of the resonances, a piezoelectric transducer (thickness 1 mm, Ferroperm Piezoceramics Pz26) was glued on the bottom of the device with conductive epoxy (Epo-Tek H20E). As proposed in earlier studies,[2,21] the piezoelectric transducer was further processed by cutting one of the two electrodes surfacially into smaller segments. The fluidic tubing for the filling with a liquid was fabricated as described by Leibacher *et al.*[15]

In order to facilitate the filling of the devices and prevent sticking of the particles on the channel walls, a minute amount of soap surfactant was added to the suspending water to lower its surface tension. Alternatively, the filling can also be eased by rendering the device hydrophilic with coatings or oxygen plasma treatment.

For the experiments, the piezoelectric transducer was excited using a function generator (Stanford Research, DS345) connected to an amplifier (ENI, 2100 L). The applied excitation voltages ranged between 20 and 30 V_{rms}, which is the same range as we reported for devices without PDMS filling.[15] This is another indication that the material damping of PDMS does not influence our experiments significantly.

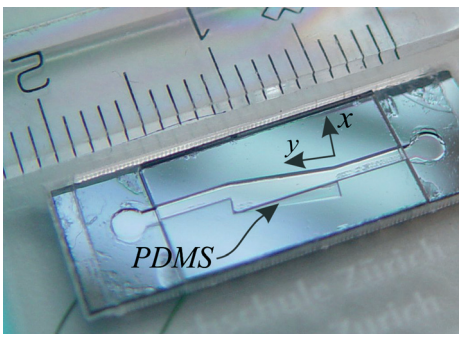

Fig. 8 Photo of a device with a triangular PDMS fill in the lower right corner of the rectangular chamber. The ruler's mm marks give a size indication.

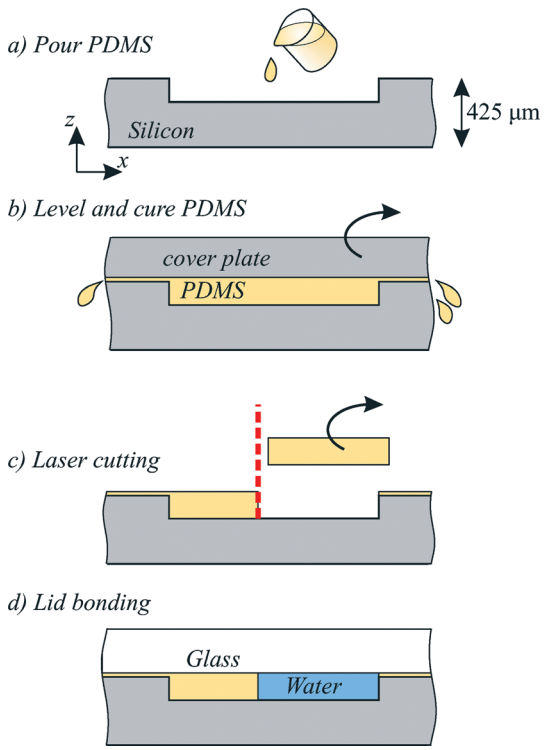

Fig. 9 Illustration of the PDMS microfabrication process steps.

3.3 Experimental results

In this section, a proof of concept shows that an ultrasonic standing wave can be generated in devices with additional PDMS layers. Then, we discuss several experiments with an application perspective.

Fig. 10 reports an experiment in a 2 mm × 6 mm rectangular microfluidic chamber. A triangle on the lower right side of the chamber was filled with PDMS. In this experiment, we chose isopropanol as the fluid, whose impedance Z_{is} is almost the same as Z_{π} (Table 1). Therefore, the acoustic field should be approximately the same as if the triangle was also filled with isopropanol instead of PDMS. Indeed, as the figure shows, an ultrasonic standing wave with 3λ in the chamber was formed at 1.574 MHz, and the 11 µm copolymer particles aligned on the 6 pressure nodal lines (particle material parameters: see Table 2). This experiment demonstrates the acoustic "transparency" of the PDMS, and it allays the concerns that the damping of PDMS might hinder the generation of a pressure field suitable for acoustophoresis. Furthermore, our manufacturing process turns out to be precise enough to result in a successful transmission of the structural vibration across the silicon–PDMS interface.

A further key experiment reports the attraction of particles towards a channel wall: in Fig. 11, 25 µm polystyrene particles suspended in water moved towards a PDMS wall by a $\lambda/2$ mode at 467 kHz. This is a result that cannot be

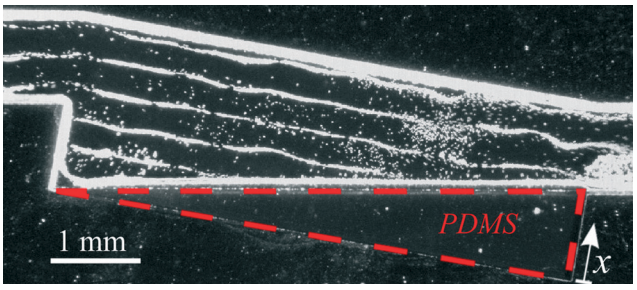

Fig. 10 Proof of concept on the example of a rectangular chamber (depth 150 µm), where a triangle on the lower right is filled with PDMS (device from Fig. 8). The 11 µm particles suspended in isopropanol aligned on 6 parallel lines at an excitation of 1.574 MHz, which shows the same behavior as that without the PDMS layer.

Table 2 Material parameters and particle properties at room temperature. f_1 and f_2 are calculated for particles in water as suspending fluid

Material	Speed of sound	Density	f_1	f_2	Diameter
Water[16]	c_{wa} = 1497 m s^{-1}	ρ_{wa} = 998 kg m^{-3}	—	—	
Copolymer[2]	c_{co} = 3000 m s^{-1}	ρ_{co} = 1050 kg m^{-3}	0.76	0.034	$2r_o$ = 11 μm and $2r_o$ = 26 μm
Polystyrene[16]	c_{ps} = 2350 m s^{-1}	ρ_{ps} = 1050 kg m^{-3}	0.61	0.034	$2r_o$ = 25 μm

achieved in conventional silicon-based acoustophoresis devices. A video of the experiment is documented in the ESI.†

The experiment shows a first application example of the PDMS boundaries for particle concentration in a flow-through mode. A flow rate of 50 μl min^{-1} was generated using a syringe pump. The particles moved towards the PDMS wall and left the device through outlet 1 in a concentrated manner. Outlet 2 is an outlet for the suspending medium, where excess liquid leaves the device. Continuous flow concentration of cells and particles is a standard task in microfluidics as reviewed by Lenshof *et al.*,[24] *e.g.* to replace centrifugation steps.

Furthermore, as mentioned in the Introduction, the attraction of particles on walls as shown here has significant biotechnological relevance.[8] The proposed device might also find applications for filtration or separation of suspended particles, similar to the applications described on the devices of Laurell *et al.*[3] Whereas these devices have to be symmetric along their *y*-axis, our device design is not restricted by this condition. This reduces the need for redundant particle outlets, which are often built to fulfill this symmetry condition.

The theoretical model for this specific configuration corresponds to section 2.2, Fig. 4 and 5. With the widths a = 0.5 mm and b = 1 mm, the $\lambda/2$ mode was expected at 421 kHz with a pressure nodal line at x = 0.11 mm. This position of the nodal line was chosen in order to prevent the particles from sticking to the wall, where the fluidic no-slip condition would result in zero flow and particle velocity. The experiment's outcome confirms the theoretical model qualitatively; however, quantitatively, the calculated frequency value is 9.9% lower than in the experiment and the pressure nodal line is close to the wall. We believe that these deviations are caused by influences of the complex three-dimensional structural and fluidic resonance mode, compliant silicon boundaries, material and manufacturing uncertainties, as well as temperature shifts[25] caused by the piezo excitation.

Fig. 12 shows a further experiment with two PDMS walls as calculated in section 2.2, Fig. 6. It demonstrates a microfluidic channel where the particles can be moved to either the left or the right channel wall. Within the manufacturing precisions, the width ratio $a:b:d$ corresponds to the analytically calculated values. The corresponding analytically calculated resonance frequencies of 513 kHz and 1076 kHz for the $\lambda/2$ and λ modes in Fig. 6 are 16% and 1% lower than in the experiments of Fig. 12a and b, respectively, which we believe to be caused by the reasons mentioned above and by imprecise fabrication of the PDMS layer widths in particular.

Cells suspended in water typically have an acoustic contrast factor of $\Phi > 0$, so their qualitative behavior is the same as that of the shown copolymer and polystyrene particles. Hence, cells and such test particles are reported to be attracted to the same locations, namely the pressure nodes.[26,27] Several research groups presented acoustophoretic cell handling with no adverse effects on their viability, whereas the cells were exposed up to 72 hours in an ultrasound field in microfluidic devices.[28,29] Furthermore, the high viability of cells in acoustophoretic devices has been reviewed recently.[30] Therefore, the shown experiments are believed to also be suitable for cell handling.

Future work might harness the described impedance matching concept for further cell handling tasks. The coupling

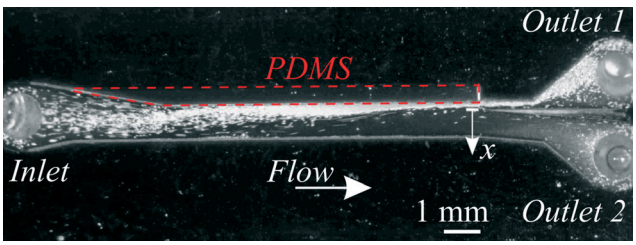

Fig. 11 Application of PDMS boundaries for particle concentration in a flow-through experiment with $\lambda/2$ mode. The microchannel has a total width of 1.5 mm in the *x*-direction and a depth of 150 μm. The upper 0.5 mm are filled with PDMS. In the lower 1 mm, water flows rightwards with suspended 25 μm particles. This PDMS boundary allows us to focus particles on the fluidic channel wall in a $\lambda/2$ mode at 467 kHz. Outlet 1 is the concentrated particle outlet, and excess suspending medium leaves through outlet 2. This experiment corresponds to the plot in Fig. 4.

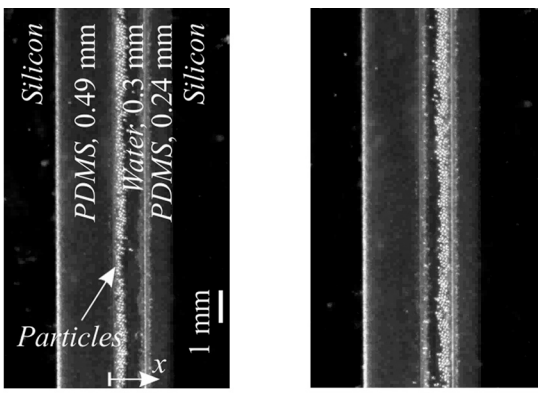

(a) left wall focused, $\lambda/2$ mode, 610 kHz (b) right wall focused, λ mode, 1090 kHz

Fig. 12 A device with a water channel (depth 60 μm) in between two PDMS layers. Focusing of 26 μm particles on the left and right channel wall is demonstrated. This experiment corresponds to the plot in Fig. 6.

of this device with further analysis and detection techniques in place or farther downstream offers additional potential.

4. Conclusions

This paper reports on novel PDMS boundaries with matched characteristic acoustic impedance in acoustophoretic microchannels. Promising applications of this PDMS boundary concept include devices which can force particles onto the microfluidic channel walls. Most conventional BAW channels in silicon have pressure antinodes on the channel wall, whereas the devices presented here allow the placement of pressure nodal lines on or even within the channel wall. Such pressure fields enable the attraction of particles onto walls, which is expected to improve various microfluidic tasks, such as particle concentration as outlined in the paper, separation of particles, particle traps, particle switches, as well as enhanced particle sensors which rely on interactions between particles and a sensor wall. Recently, Wiklund *et al.*[8] formulated the need for such cell/particle attracting walls in microsystems: in combination with immuno-selective agents coated on biosensor surfaces, the acoustophoretic movement of cells or antigen-coated particles towards these sensing surfaces offers promising novel detection capabilities for biotechnological applications.

PDMS has acoustic properties which are similar to water. Therefore, when it is introduced in a microfluidic chamber, the acoustic field remains approximately the same as that without the PDMS filling. This acoustic "transparency" allows more freedom with respect to the acoustic field design: in conventional microfluidic channels, the walls are both the fluidic and the acoustic boundary. With a PDMS filling, these two functions can be decoupled: the silicon walls are still the acoustic boundaries, whereas the PDMS filling can define an arbitrary fluidic boundary. We believe that these findings can expand the possibilities of acoustofluidic devices.

Acknowledgements

The authors would like to express their gratitude for the support of the whole institute and the funding by ETH Zurich and the Swiss National Science Foundation, SNF no. 200021_126986.

References

1 O. Manneberg, B. Vanherberghen, B. Onfelt and M. Wiklund, *Lab Chip*, 2009, **9**, 833–837.
2 S. Oberti, A. Neild and J. Dual, *J. Acoust. Soc. Am.*, 2007, **121**, 778–785.
3 T. Laurell, F. Petersson and A. Nilsson, *Chem. Soc. Rev.*, 2007, **36**, 492–506.
4 D. Hartono, Y. Liu, P. L. Tan, X. Y. S. Then, L.-Y. L. Yung and K.-M. Lim, *Lab Chip*, 2011, **11**, 4072–4080.
5 H. Bruus, J. Dual, J. Hawkes, M. Hill, T. Laurell, J. Nilsson, S. Radel, S. Sadhal and M. Wiklund, *Lab Chip*, 2011, **11**, 3579–3580.
6 A. Lenshof, M. Evander, T. Laurell and J. Nilsson, *Lab Chip*, 2012, **12**, 684–695.
7 I. Leibacher, S. Schatzer and J. Dual, *Proceedings of the 17th International Conference on Miniaturized Systems for Chemistry and Life Sciences, 27–31 October 2013*, Freiburg, Germany, 2013, 757759.
8 M. Wiklund, S. Radel and J. J. Hawkes, *Lab Chip*, 2012, **12**, 4667–4676.
9 P. Glynne-Jones, R. J. Boltryk and M. Hill, *Lab Chip*, 2012, **12**, 1417–1426.
10 P. Glynne-Jones, R. J. Boltryk, M. Hill, N. R. Harris and P. Baclet, *J. Acoust. Soc. Am.*, 2009, **126**, EL75–EL79.
11 X. Ding, S.-C. S. Lin, B. Kiraly, H. Yue, S. Li, I.-K. Chiang, J. Shi, S. J. Benkovic and T. J. Huang, *Proc. Natl. Acad. Sci. U. S. A.*, 2012, **109**, 11105–11109.
12 L. P. Gor'kov, *Sov. Phys. - Dokl.*, 1962, **6**, 773–775.
13 K. Yosioka and Y. Kawasima, *Acustica*, 1955, **5**, 167–173.
14 H. Bruus, *Lab Chip*, 2012, **12**, 1014–1021.
15 I. Leibacher, W. Dietze, P. Hahn, J. Wang, S. Schmitt and J. Dual, *Microfluid. Nanofluid.*, 2013, DOI: 10.1007/s10404-013-1240-7.
16 H. Bruus, *Lab Chip*, 2012, **12**, 20–28.
17 L. E. Kinsler, A. R. Frey, A. B. Coppens and J. V. Sanders, *Fundamentals of Acoustics*, John Wiley & Sons, 3rd edn, 1982.
18 P. Glynne-Jones, R. J. Boltryk, N. R. Harris, A. W. Cranny and M. Hill, *Ultrasonics*, 2010, **50**, 68–75.
19 B. Hartmann and J. Jarzynski, *J. Acoust. Soc. Am.*, 1974, **56**, 1469–1477.
20 H.-B. Liu and H.-Q. Gong, *J. Micromech. Microeng.*, 2009, **19**, 037002.
21 A. Neild, S. Oberti and J. Dual, *Sens. Actuators, B*, 2007, **121**, 452–461.
22 A. Rodríguez, J. Canosa and J. Tojo, *J. Chem. Eng. Data*, 2001, **46**, 1476–1486.
23 H. J. McSkimin and J. P. Andreatch, *J. Appl. Phys.*, 1964, **35**, 2161–2165.
24 A. Lenshof, C. Magnusson and T. Laurell, *Lab Chip*, 2012, **12**, 1210–1223.
25 P. Augustsson, R. Barnkob, S. T. Wereley, H. Bruus and T. Laurell, *Lab Chip*, 2011, **11**, 4152–4164.
26 A. Haake, A. Neild, D.-H. Kim, J.-E. Ihm, Y. Sun, J. Dual and B.-K. Ju, *Ultrasound Med. Biol.*, 2005, **31**, 857–864.
27 A. Neild, S. Oberti, G. Radziwill and J. Dual, *Biotechnol. Bioeng.*, 2007, **97**, 1335–1339.
28 M. Evander and J. Nilsson, *Lab Chip*, 2012, **12**, 4667–4676.
29 B. Vanherberghen, O. Manneberg, A. Christakou, T. Frisk, M. Ohlin, H. M. Hertz, B. Onfelt and M. Wiklund, *Lab Chip*, 2010, **10**, 2727–2732.
30 M. Wiklund, *Lab Chip*, 2012, **12**, 2018–2028.

